

## Article

# Methylene Blue-Loaded Mesoporous Silica-Coated Gold Nanorods on Graphene Oxide for Synergistic Photothermal and Photodynamic Therapy

Sun-Hwa Seo, Ara Joe, Hyo-Won Han, Panchanathan Manivasagan  and Eue-Soon Jang \*

Department of Applied Chemistry, Kumoh National Institute of Technology, Gumi 730-701, Gyeongbuk, Korea  
\* Correspondence: euesoon@kumoh.ac.kr

**Abstract:** Photo-nanotheranostics integrates near-infrared (NIR) light-triggered diagnostics and therapeutics, which are combined into a novel all-in-one phototheranostic nanomaterial that holds great promise for the early detection and precise treatment of cancer. In this study, we developed methylene blue-loaded mesoporous silica-coated gold nanorods on graphene oxide (MB-GNR@mSiO<sub>2</sub>-GO) as an all-in-one photo-nanotheranostic agent for intracellular surface-enhanced Raman scattering (SERS) imaging-guided photothermal therapy (PTT)/photodynamic therapy (PDT) for cancer. Amine functionalization of the MB-GNR@mSiO<sub>2</sub> surfaces was performed using 3-aminopropyltriethoxysilane (APTES), which was well anchored on the carboxyl groups of graphene oxide (GO) nanosheets uniformly, and showed a remarkably higher photothermal conversion efficiency (48.93%), resulting in outstanding PTT/PDT for cancer. The in vitro photothermal/photodynamic effect of MB-GNR@mSiO<sub>2</sub>-GO with laser irradiation showed significantly reduced cell viability (6.32%), indicating that MB-GNR@mSiO<sub>2</sub>-GO with laser irradiation induced significantly more cell deaths. Under laser irradiation, MB-GNR@mSiO<sub>2</sub>-GO showed a strong SERS effect, which permits accurate cancer cell detection by SERS imaging. Subsequently, the same Raman laser can focus on highly detected MDA-MB-231 cells for a prolonged time to perform PTT/PDT. Therefore, MB-GNR@mSiO<sub>2</sub>-GO has great potential for precise SERS imaging-guided synergistic PTT/PDT for cancer.

**Keywords:** methylene blue; gold nanorods; graphene oxide; diagnosis; phototherapy



**Citation:** Seo, S.-H.; Joe, A.; Han, H.-W.; Manivasagan, P.; Jang, E.-S. Methylene Blue-Loaded Mesoporous Silica-Coated Gold Nanorods on Graphene Oxide for Synergistic Photothermal and Photodynamic Therapy. *Pharmaceutics* **2022**, *14*, 2242. <https://doi.org/10.3390/pharmaceutics14102242>

Academic Editor: Natasa Skalko-Basnet

Received: 25 August 2022

Accepted: 18 October 2022

Published: 20 October 2022

**Publisher's Note:** MDPI stays neutral with regard to jurisdictional claims in published maps and institutional affiliations.



**Copyright:** © 2022 by the authors. Licensee MDPI, Basel, Switzerland. This article is an open access article distributed under the terms and conditions of the Creative Commons Attribution (CC BY) license (<https://creativecommons.org/licenses/by/4.0/>).

## 1. Introduction

Cancer is a leading cause of human death globally, and exploiting photo-nanotheranostics is an urgent requirement for cancer treatment [1,2]. Photo-nanotheranostics is the integration of near-infrared (NIR) light-triggered diagnostics and therapeutics, which are combined into a new all-in-one nanomaterial that has great potential for accurate cancer diagnosis and effective phototherapy [3]. As an emerging photo-triggered diagnostic technique, surface-enhanced Raman scattering (SERS) imaging has been increasingly considered a promising diagnostic method for the development of theranostic systems because of its high sensitivity, enhanced photostability, and multiplexing abilities [4]. SERS has emerged as an effective imaging method for accurate cancer detection [5]. As emerging phototherapeutic strategies, photothermal therapy (PTT) and photodynamic therapy (PDT) have attracted increasing clinical attention in recent years, which is beneficial for enhanced cancer therapy because of their synergistic effects [6]. PTT has attracted considerable interest in cancer treatment because of its minimal invasiveness, high efficiency, low toxicity, and deep tissue penetration [7,8]. In PTT, a photothermal nanoagent directly converts the absorbed NIR light into heat-to-kill cancer cells [9]. PDT has attracted much attention as a less invasive therapeutic modality for treating cancer. It employs photosensitizers (PSs) and light irradiation at certain wavelengths of photon energy to produce reactive oxygen species (ROS), including singlet oxygen (<sup>1</sup>O<sub>2</sub>), to destroy cancer cells [7]. Therefore, the

integration of SERS imaging, PTT, and PDT treatment into one system could provide a new photo-nanotheranostic platform for precise cancer diagnosis and therapy [6].

To date, various nanoparticles (NPs) with strong NIR absorption properties and an effective heat transfer mechanism have been developed as photo-nanotheranostic agents for SERS imaging-guided phototherapy, including polymer NPs [10], carbon NPs [11], copper sulfide NPs [12], and gold nanostructures [13]. Among these photothermal nanomaterials, gold nanorods (GNRs) have emerged as interesting nanomaterials for theranostic applications, including drug delivery, PTT, SERS imaging, and photoacoustic imaging, because of their excellent small size, biocompatibility, ease of synthesis, ease of surface modification, and strong tunable extinction in the NIR region (600–1100 nm) [14]. The seed-mediated method has become one of the most powerful and versatile methods for the synthesis of GNRs due to its advantages, such as a simple process and high yield of GNRs [15,16]. GNRs have proven to be appropriate candidates for SERS imaging-guided PTT because of their strong SERS effects and high photothermal conversion properties [17]. However, GNRs with nonporous structures have the poor dye-loading capacity, which seriously limits their efficacy in PDT [18]. The Stöber method is a widely used method for obtaining silica-coated NPs due to its advantages, such as ease of synthesis, low cost, mild reaction conditions, and a broad range of achievable particle sizes [19,20]. Mesoporous silica (mSiO<sub>2</sub>) is highly suitable as a coating material for GNRs [21]. Mesoporous silica-coated gold nanorods (GNR@mSiO<sub>2</sub>) show great potential for theranostic applications because of their high specific surface area, high accessibility, tunable pore size and volume, high dye loading capability, high stability, well-defined surface properties, and excellent biocompatibility [22]. Methylene blue (MB) is a water-soluble, Food and Drug Administration (FDA)-approved, and photosensitizer (PS) drug that is frequently used in PDT to treat cancerous and non-cancerous diseases [23]. MB has high levels of ROS, such as singlet oxygen (<sup>1</sup>O<sub>2</sub>) quantum yield, under laser light exposure [24]. MB was directly loaded with high loading capability inside the pores of mSiO<sub>2</sub> to obtain MB-GNR@mSiO<sub>2</sub> [25]. Most importantly, the integration of GNRs with other NPs, such as graphene oxide (GO) is being actively pursued because of its enhanced photothermal conversion property when compared with single NPs [3]. GO is a sheet-like two-dimensional layer of carbon nanomaterials and is the most attractive material for the PTT of cancer because of its excellent biocompatibility, conductivity, large surface area, stability, facile surface functionalization, and high optical absorption coefficient in the NIR region [26]. Therefore, the integration of MB-GNR@mSiO<sub>2</sub> with GO is a promising strategy for achieving high PTT efficacy because of its synergistic effect [9]. In this study, we developed multifunctional MB-GNR@mSiO<sub>2</sub>-GO as a novel photo-nanotheranostic agent for SERS imaging-guided synergistic PTT/PDT.

## 2. Materials and Methods

### 2.1. Materials

All the materials and reagents were purchased from Sigma-Aldrich (St. Louis, MO, USA) and used without further purification.

### 2.2. Synthesis of MB-GNR@mSiO<sub>2</sub>-GO

Gold nanorods (GNRs) were prepared in an aqueous cetyltrimethylammonium bromide (CTAB) solution using a seed-mediated method [15]. For the mesoporous silica (mSiO<sub>2</sub>) coating on the surface of GNRs (GNR@mSiO<sub>2</sub>), GNR@mSiO<sub>2</sub> was synthesized according to a previously published procedure, with minor modifications [27,28]. Briefly, 10 mL of the purified GNR solution was added to 5 mL of absolute ethanol and 5 mL of deionized water (DW), and the mixture was stirred for 3 h at ambient temperature. Subsequently, 200 µL of NaOH solution (0.1 M) was slowly added dropwise with stirring. Subsequently, 60 µL of tetraethyl orthosilicate (TEOS; 20%) in methanol solution was added three times at 30 min intervals with gentle stirring. The mixture was allowed to react for 2 days at 30 °C with vigorous stirring. Mesoporous silica-coated GNRs (GNR@mSiO<sub>2</sub>) were collected by centrifugation at 15,000 rpm for 30 min and washed thrice with ethanol. The

purified GNR@mSiO<sub>2</sub> samples obtained were redispersed in 10 mL of ethanol for further experiments. Methylene blue (MB) loaded onto GNR@mSiO<sub>2</sub> was prepared according to previous reports [25]. MB (0.1 mg) was added to 10 mL of purified GNR@mSiO<sub>2</sub>, and the reaction solution was then stirred for 2 days at 25 °C, which was covered with aluminum foil to avoid light exposure and to protect the fluorescent dyes from photodegradation. The reaction solutions (MB-GNR@mSiO<sub>2</sub>) were separated by centrifugation and washed repeatedly with DW until the supernatant changed from dark blue to colorless.

For the conjugation of amine functional groups on the surface of MB-GNR@mSiO<sub>2</sub>, 1 mL of 3-aminopropyltriethoxysilane (APTES) was mixed with 10 mL of MB-GNR@mSiO<sub>2</sub> and stirred for 6 h at ambient temperature. The reaction solutions were centrifuged and washed thrice using DW. The aminated MB-GNR@mSiO<sub>2</sub>-APTES was re-dispersed in DW for further experiments. GO was prepared using a modified Hummers' method [29]. The primary amino groups of MB-GNR@mSiO<sub>2</sub>-APTES (5.0 mL) were reacted with the carboxyl groups of GO (0.1 mg) via a coupling reaction in the presence of 1-ethyl-3-(3-dimethylaminopropyl) carbodiimide hydrochloride (EDC; 1.0 mg) and *N*-hydroxysuccinimide (NHS; 1.0 mg) with overnight stirring at room temperature. The amino group of MB-GNR@mSiO<sub>2</sub>-APTES can be easily cross-linked with the carboxyl group of GO, and MB-GNR@mSiO<sub>2</sub>-GO can potentially prevent the leaching of MB from the mesopores of SiO<sub>2</sub>. The reaction solutions (MB-GNR@mSiO<sub>2</sub>-GO) were centrifuged, washed repeatedly using DW to eliminate unreacted reactants, and freeze-dried.

### 2.3. Characterization

The UV–vis spectra of GNR, GNR@mSiO<sub>2</sub>, MB-GNR@mSiO<sub>2</sub>, free GO, and MB-GNR@mSiO<sub>2</sub>-GO were obtained using a Shimadzu (Kyoto, Japan) UV-2600 UV–vis spectrophotometer. The morphologies of the nanomaterials were characterized using a Cs-corrected field emission transmission electron microscope (Cs-corrected FE-TEM; JEM-ARM-200F, JEOL, Tokyo, Japan) equipped with energy-dispersive X-ray spectroscopy (EDX). The particle size range and zeta potential (ZP) of the nanomaterials were measured using a particle size and ZP analyzer (90 Plus, Brookhaven Instruments, Holtsville, NY, USA). Raman spectra at 785 nm (2 mW, spot area = 2–100 μm) were obtained using a Renishaw inVia Raman spectrometer (Gloucestershire, UK) equipped with a Leica DM 2500 microscope with 1200 g/mm grating. The final gold (Au) ion concentration of the nanomaterials in aqueous solutions was determined to be 36 μg Au/mL by inductively coupled plasma optical emission spectroscopy (ICP-OES, Santa Clara, CA, USA). The photothermal experiments were carried out using an NIR laser at 785 nm (Changchun New Industries Optoelectronics Technology, Changchun, China; power density: 0.8 W/cm<sup>2</sup>, laser beam diameter: 4 mm, laser beam shape: round), and infrared (IR) thermal images were captured every 1 s using an FLIR CX-Series compact thermal imaging camera. A transparent cuvette was filled with a known concentration of NP solutions and the top surface was fixed with a laser pointer lens. An IR thermal camera was placed at a 30 cm distance to capture a lateral image of the cuvette and a laser.

### 2.4. Measurement of Photothermal Performance

One milliliter of each of the GNR, GNR@mSiO<sub>2</sub>, MB-GNR@mSiO<sub>2</sub>, GO, and MB-GNR@mSiO<sub>2</sub>-GO aqueous solutions (36 μg/mL) was added to a quartz cuvette and exposed to a 785 nm NIR laser at 0.8 W/cm<sup>2</sup> for 25 min. The temperature profiles were recorded every 1 s using an FLIR CX-Series compact thermal imaging camera. Additionally, the gold concentration of the MB-GNR@mSiO<sub>2</sub>-GO was calculated to be 36 μg Au/mL and different volumes (0–200 μL of 36 μg/mL) of the MB-GNR@mSiO<sub>2</sub>-GO aqueous solutions (1 mL) were added to a quartz cuvette and exposed to a 785 nm laser at 0.8 W/cm<sup>2</sup> for 25 min. Temperature profiles and infrared (IR) thermal images were obtained using a FLIR thermal imaging camera. To evaluate the photothermal stability of MB-GNR@mSiO<sub>2</sub>-GO, the MB-GNR@mSiO<sub>2</sub>-GO (200 μL of 36 μg/mL) aqueous solution was filled in a quartz cuvette and then exposed to four cycles of laser on/off (785 nm, 0.8 W/cm<sup>2</sup>). The UV–vis

spectra of MB-GNR@mSiO<sub>2</sub>-GO were recorded and characterized using TEM, DLS, and ZP after four cycles of laser irradiation. The photothermal conversion efficiency ( $\eta$ ) of MB-GNR@mSiO<sub>2</sub>-GO (200  $\mu$ L of 36  $\mu$ g/mL) was calculated according to the thermal balance using the following Equation (1), as described in previous reports [30,31].

$$\eta = \frac{hS(T_{Max} - T_{Sur}) - Q_{dis}}{I(1 - 10^{-A_{808}})} \quad (1)$$

### 2.5. Cells Culture

The mouse muscle fibroblast cell line (BLO-11) and human breast cancer cell line (MDA-MB-231 cells) were purchased from the Korean Cell Line Bank (Seoul, Korea). The BLO-11 and MDA-MB-231 cells were cultured in Dulbecco's modified Eagle's medium (DMEM) with 1% antibiotics (penicillin/streptomycin) and 10% fetal bovine serum (FBS) at 37 °C under 5% CO<sub>2</sub>.

### 2.6. In Vitro PTT/PDT Synergistic Effect

The in vitro photothermal/photodynamic effects of GNR, MB-GNR@mSiO<sub>2</sub>, GO, and MB-GNR@mSiO<sub>2</sub>-GO against normal (BLO-11) and cancer (MDA-MB-231) cells were evaluated using the 3-(4,5-dimethylthiazol-2-yl)-2,5-diphenyltetrazolium bromide (MTT) assay. BLO-11 and MDA-MB-231 cells (7000 cells/well) were seeded in 96-well plates and cultured at 37 °C for 24 h. The cells were incubated with GNR, MB-GNR@mSiO<sub>2</sub>, GO, and MB-GNR@mSiO<sub>2</sub>-GO (200  $\mu$ L of 36  $\mu$ g/mL) for 12 h and 48 h and then irradiated with a 785 nm laser at 0.8 W/cm<sup>2</sup> for various time points (0, 10, 30, and 50 min). The cells were treated with all the nanomaterials and were incubated with a 785 nm laser irradiation as the control. All cells were further incubated for 6 h, and cell viability was evaluated using the MTT assay. The percentage of cell viability was determined by the following Formula (2):

$$\text{Percentage of cell viability (\%)} = \frac{\text{OD value of samples}}{\text{OD value of controls}} \times 100 \quad (2)$$

To further confirm the in vitro photothermal/photodynamic effect of GNR, MB-GNR@mSiO<sub>2</sub>, and MB-GNR@mSiO<sub>2</sub>-GO, the MDA-MB-231 cells were stained using calcein-AM and propidium iodide (PI) to visually identify live (green) and dead (red) cells. The MDA-MB-231 cells were cultured in 6-well plates and incubated overnight at 37 °C. After incubation, the cells were treated with GNR, MB-GNR@mSiO<sub>2</sub>, and MB-GNR@mSiO<sub>2</sub>-GO (200  $\mu$ L of 36  $\mu$ g/mL) for 12 h and irradiated with a 785 nm laser (0.8 W/cm<sup>2</sup>) for various time points (0, 10, 30, and 50 min). Then, all cells were incubated for 6 h and stained using calcein-AM and PI for 30 min. Finally, the cells were imaged using a confocal fluorescence microscope (Nikon Confocal A1R; Nikon, Tokyo, Japan).

To quantify intracellular ROS, MDA-MB-231 cells were cultured in 6-well plates and incubated for 24 h at 37 °C. The MDA-MB-231 cells were then incubated with GNR, MB-GNR@mSiO<sub>2</sub>, and MB-GNR@mSiO<sub>2</sub>-GO (200  $\mu$ L of 36  $\mu$ g/mL) for 12 h and exposed to a 785 nm laser at 0.8 W/cm<sup>2</sup> for various time points (0, 10, 30, and 50 min). The cells were incubated for another 6 h and stained with 2,7-Dichlorofluorescein diacetate (DCFH-DA 10  $\mu$ M) for 30 min. DCFH-DA is a non-fluorescent dye used to detect PDT-induced intracellular ROS production. The cells were washed with PBS and imaged using a confocal fluorescence microscope (Nikon Confocal A1R; Nikon, Tokyo, Japan).

### 2.7. SERS Imaging Measurement

The SERS imaging measurement was recorded with a Renishaw inVia Raman spectrometer (Gloucestershire, UK) equipped with a NIR laser (785 nm, 2 mW, spot area = 2–100  $\mu$ m) and a Leica DM 2500 microscope with 1200 g/mm grating, which was focused for 40 s on the samples through a 20 $\times$  microscope objective. MDA-MB-231 cells were grown on a chambered slide glass at 37 °C for 24 h and then cells were treated with GNR

(control), MB-GNR@mSiO<sub>2</sub>, and MB-GNR@mSiO<sub>2</sub>-GO. After incubation, the slide glass was performed using a Renishaw inVia Raman microscope.

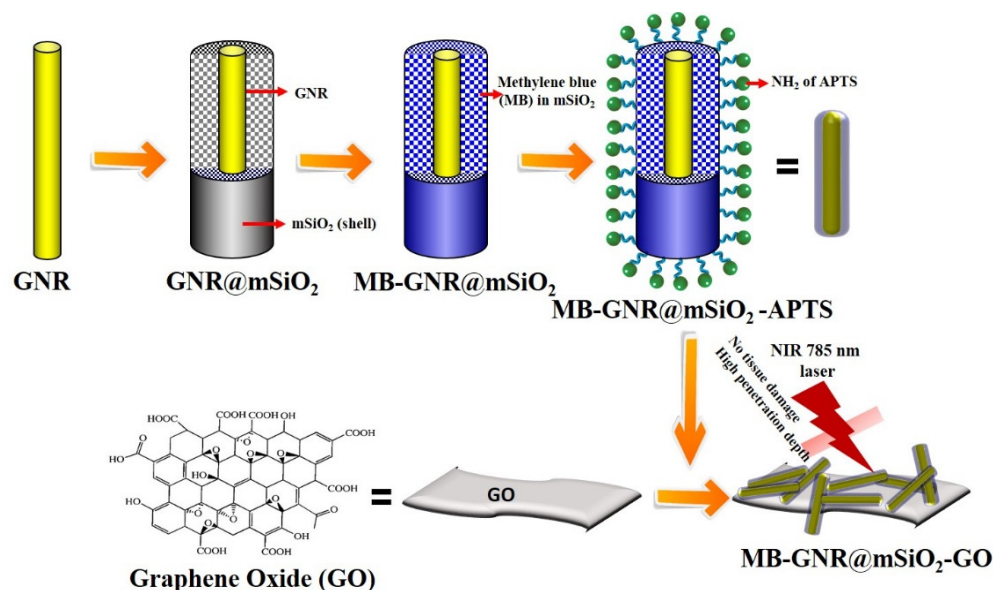
### 2.8. Statistical Analysis

Data were expressed as mean ± standard deviation (SD) in at least three trials. The significant difference between groups was performed using a Student's two-tailed *t*-test and one-way ANOVA with SPSS software 23.0. \* *p* < 0.05 and \*\* *p* < 0.01 were statistically significant.

## 3. Results and Discussion

### 3.1. Synthesis and Characterization of MB-GNR@mSiO<sub>2</sub>-GO

The preparation process of MB-GNR@mSiO<sub>2</sub>-GO for PTT/PDT is illustrated in Scheme 1. GNRs were prepared in an aqueous CTAB solution using a seed-mediated growth method [15]. The synthesized GNRs were covered with a mesoporous layer of silica (mSiO<sub>2</sub>) using a previously reported method, forming highly monodisperse GNR@mSiO<sub>2</sub> [27,28]. MB was directly loaded inside the pores of mSiO<sub>2</sub> with a high loading capacity to obtain MB-GNR@mSiO<sub>2</sub> [25]. Amine functionalization of the MB-GNR@mSiO<sub>2</sub> surfaces was performed using APTES as a silane coupling agent (MB-GNR@mSiO<sub>2</sub>-APTES). GO was synthesized using a modified Hummers' method [29]. Finally, the carboxyl groups of GO were covalently conjugated to the free amino groups of MB-GNR@mSiO<sub>2</sub>-APTES through a coupling reaction in the presence of EDC/NHS chemistry to form MB-GNR@mSiO<sub>2</sub>-GO, which can potentially prevent leaching of the loaded MB molecules before MB-GNR@mSiO<sub>2</sub>-GO is taken up by the cells [32].



**Scheme 1.** Schematic illustration of the synthesis process of methylene blue-loaded mesoporous silica-coated gold nanorods on graphene oxide (MB-GNR@mSiO<sub>2</sub>-GO) for photothermal and photodynamic therapy.

The morphologies of GNR, GNR@mSiO<sub>2</sub>, MB-GNR@mSiO<sub>2</sub>, GO, and MB-GNR@mSiO<sub>2</sub>-GO were characterized using Cs-corrected FE-TEM (Figure 1). The GNRs have a uniform and well-defined rod-like structure with an average length of  $47 \pm 3.6$  nm and a diameter of  $12 \text{ nm} \pm 2.4$  nm. The GNRs were coated with mSiO<sub>2</sub> to form highly monodispersed GNR@mSiO<sub>2</sub>. The thickness of the mSiO<sub>2</sub> was 38 nm, and a nanoporous structure could be observed. Similar findings were reported by Xia et al., who demonstrated that the thickness of the GNR@mSiO<sub>2</sub> was 12 nm [33]. After loading with MB, MB-GNR@mSiO<sub>2</sub> exhibited a uniform size and morphology. The as-prepared GO was nanosheet-shaped with a smooth surface and wrinkled edges. MB-GNR@mSiO<sub>2</sub> was uniformly anchored on the

GO nanosheets (Figure S1). Additionally, Cs-corrected FE-TEM and the corresponding EDX mapping of MB-GNR@mSiO<sub>2</sub>-GO revealed the presence of Au, Si, S, C, and O, confirming the presence of MB-GNR@mSiO<sub>2</sub>-GO (Figure 2).

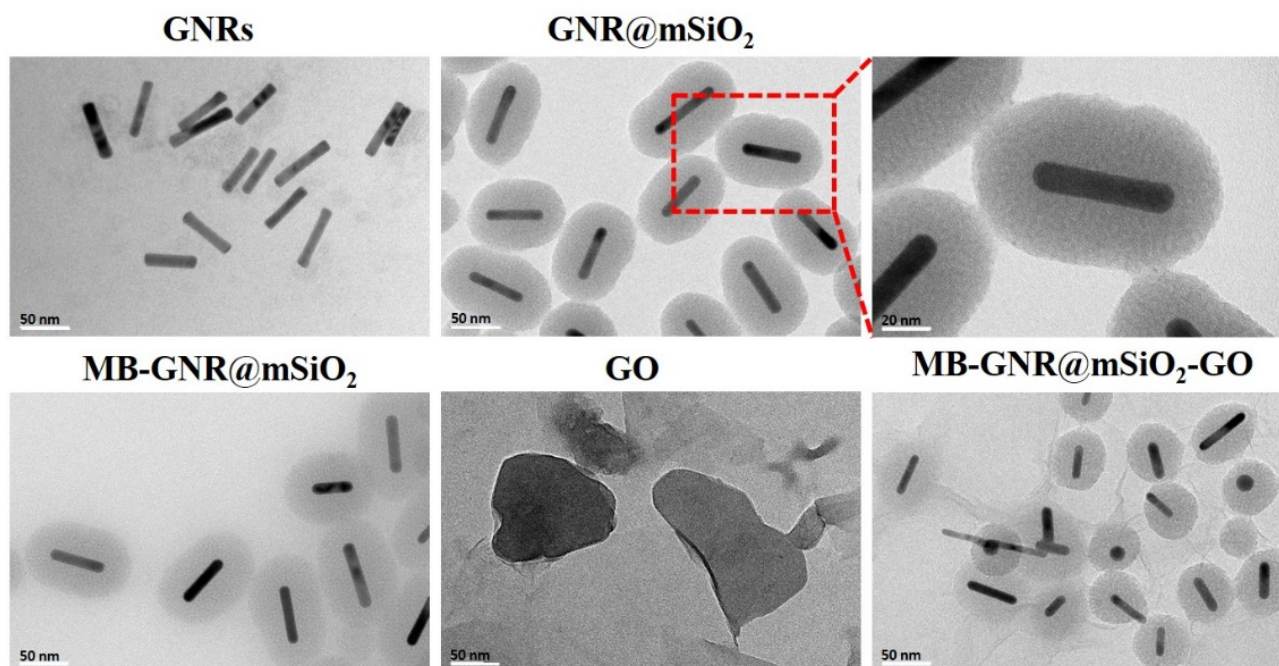


**Figure 1.** FETEM images of gold nanorods (GNRs), mesoporous silica-coated gold nanorods (GNR@mSiO<sub>2</sub>), methylene blue-loaded mesoporous silica-coated gold nanorods (MB-GNR@mSiO<sub>2</sub>), graphene oxide (GO), and methylene blue-loaded mesoporous silica-coated gold nanorods on graphene oxide (MB-GNR@mSiO<sub>2</sub>-GO).

Figure 3a shows the UV-vis spectra of GNR, GNR@mSiO<sub>2</sub>, MB-GNR@mSiO<sub>2</sub>, GO, and MB-GNR@mSiO<sub>2</sub>-GO. The as-prepared GNR has a strong longitudinal surface plasmon resonance (LSPR) peak at 800 nm, which is more suitable for PTT with an NIR laser [34]. After coating with SiO<sub>2</sub>, the LSPR peak of GNR@mSiO<sub>2</sub> was slightly red-shifted to 810 nm, which could be attributed to an increase in the local refractive index of the surrounding medium after the creation of the silica shell layer by replacing the CTAB [35]. After loading with MB, the absorption spectra of MB-GNR@mSiO<sub>2</sub> showed a characteristic peak of MB at 655 nm and a strong LSPR peak at 800 nm, indicating that MB molecules were successfully loaded onto GNR@mSiO<sub>2</sub> and were highly effective in PDT, owing to their ability to generate ROS [36]. The absorption spectrum of GO spanned from the UV-vis range to the NIR range, which can effectively enhance the photothermal conversion efficiency [37]. The absorption spectra of MB-GNR@mSiO<sub>2</sub>-GO exhibited characteristic peaks of GO, MB, and GNR@mSiO<sub>2</sub> at 280, 655, and 810 nm, respectively, confirming their strong photothermal and photodynamic properties.

The particle sizes of GNR, GNR@mSiO<sub>2</sub>, MB-GNR@mSiO<sub>2</sub>, GO, and MB-GNR@mSiO<sub>2</sub>-GO were measured by dynamic light scattering (DLS). The GNR, GNR@mSiO<sub>2</sub>, MB-GNR@mSiO<sub>2</sub>, GO, and MB-GNR@mSiO<sub>2</sub>-GO have average sizes of  $43.67 \pm 2.18$  nm,  $188.46 \pm 3.42$  nm,  $196.57 \pm 4.17$  nm,  $80.47 \pm 4.02$  nm, and  $294.90 \pm 2.74$  nm, respectively (Figure 3b). The average particle size of GNR@mSiO<sub>2</sub> increased to  $\sim 144.79$  nm when compared with GNR, indicating that the mSiO<sub>2</sub> layer was effectively coated on the surface of the GNR. The average particle size of MB-GNR@mSiO<sub>2</sub> also increased to  $\sim 8.11$  nm compared with GNR@mSiO<sub>2</sub>, demonstrating that MB was successfully loaded onto GNR@mSiO<sub>2</sub>. Additionally, the particle size of MB-GNR@mSiO<sub>2</sub>-GO increased significantly to  $\sim 98.33$  nm, implying that GO was covalently conjugated to MB-GNR@mSiO<sub>2</sub>. As shown in Figure 3c, the zeta potentials (ZP) of GNR, GNR@mSiO<sub>2</sub>, MB, MB-GNR@mSiO<sub>2</sub>, GO,

and MB-GNR@mSiO<sub>2</sub>-GO were measured in PBS (pH 7.4). The ZP of GNR was  $+35.4 \pm 2.0$  mV due to the presence of positively charged CTAB on the surface of GNR. The ZP of GNR@mSiO<sub>2</sub> was  $-31.0 \pm 1.5$  mV because of the hydroxyl groups on the surface of GNR@mSiO<sub>2</sub>. The ZP of MB was  $+7.5 \pm 0.4$  mV because of the positively charged blue dye. After MB loading, the ZP of MB-GNR@mSiO<sub>2</sub> was  $-31.4 \pm 2.0$  mV because the positively charged MB can be easily absorbed on the mSiO<sub>2</sub>, which indicated the successful loading of MB and GNR@mSiO<sub>2</sub>. The ZP of GO was  $-34.0 \pm 2.0$  mV because of the ionized carboxylic acid groups. The ZP of MB-GNR@mSiO<sub>2</sub>-GO was  $-39.0 \pm 2.0$  mV which confirmed the successful conjugation of GO and MB-GNR@mSiO<sub>2</sub>-GO [38].

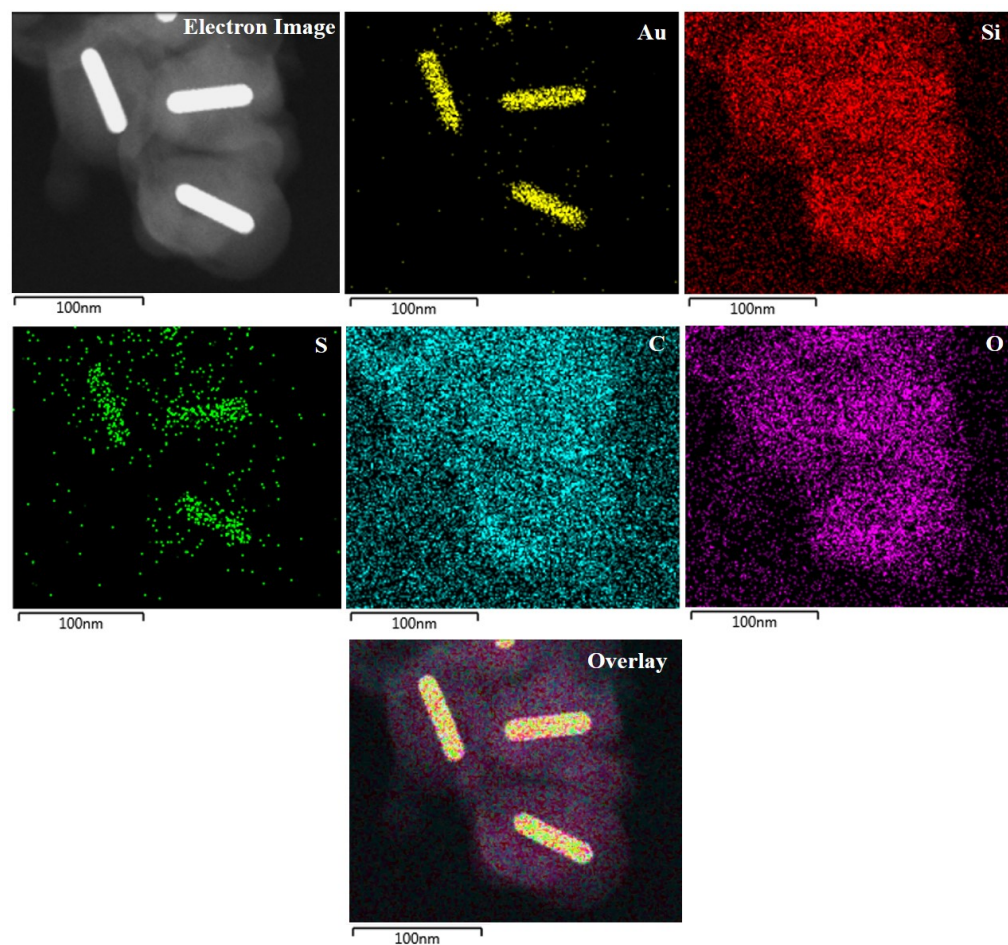


**Figure 2.** Cs-corrected field emission transmission electron microscope (Cs-corrected FE-TEM) image of methylene blue-loaded mesoporous silica-coated gold nanorods on graphene oxide (MB-GNR@mSiO<sub>2</sub>-GO) and corresponding energy-dispersive X-ray (EDX) mapping of MB-GNR@mSiO<sub>2</sub>-GO.

The micro-Raman spectra of the synthesized GNR, MB-GNR@mSiO<sub>2</sub>, and MB-GNR@mSiO<sub>2</sub>-GO were analyzed using an excitation laser at 785 nm (2 mW, spot area = 2–100  $\mu$ m) and are shown in Figure 3d. Strong Raman signals were recorded for MB-GNR@mSiO<sub>2</sub> and MB-GNR@mSiO<sub>2</sub>-GO, while GNR did not show any Raman signals. The Raman spectra of MB-GNR@mSiO<sub>2</sub> and MB-GNR@mSiO<sub>2</sub>-GO showed intense bands at 246 cm<sup>-1</sup>, 445 cm<sup>-1</sup>, 771 cm<sup>-1</sup>, 1317 cm<sup>-1</sup>, 1397 cm<sup>-1</sup>, and 1624 cm<sup>-1</sup>, assigned to the Au–N stretching mode ( $\nu$ (Au–N)), C–N–C skeletal deformation mode ( $\delta$ (C–N–C)),  $\gamma$ (C–H) stretching mode,  $\nu$ (N–CH<sub>3</sub>) mode,  $\nu_{\text{sym}}$ (C–N) mode, and  $\nu$ (C–C)<sub>ring</sub> mode, respectively. The Raman spectra of MB-GNR@mSiO<sub>2</sub>-GO were much stronger than those of MB-GNR@mSiO<sub>2</sub>, suggesting that GO has a high binding affinity for the MB-GNR@mSiO<sub>2</sub> surface [25,28,39].

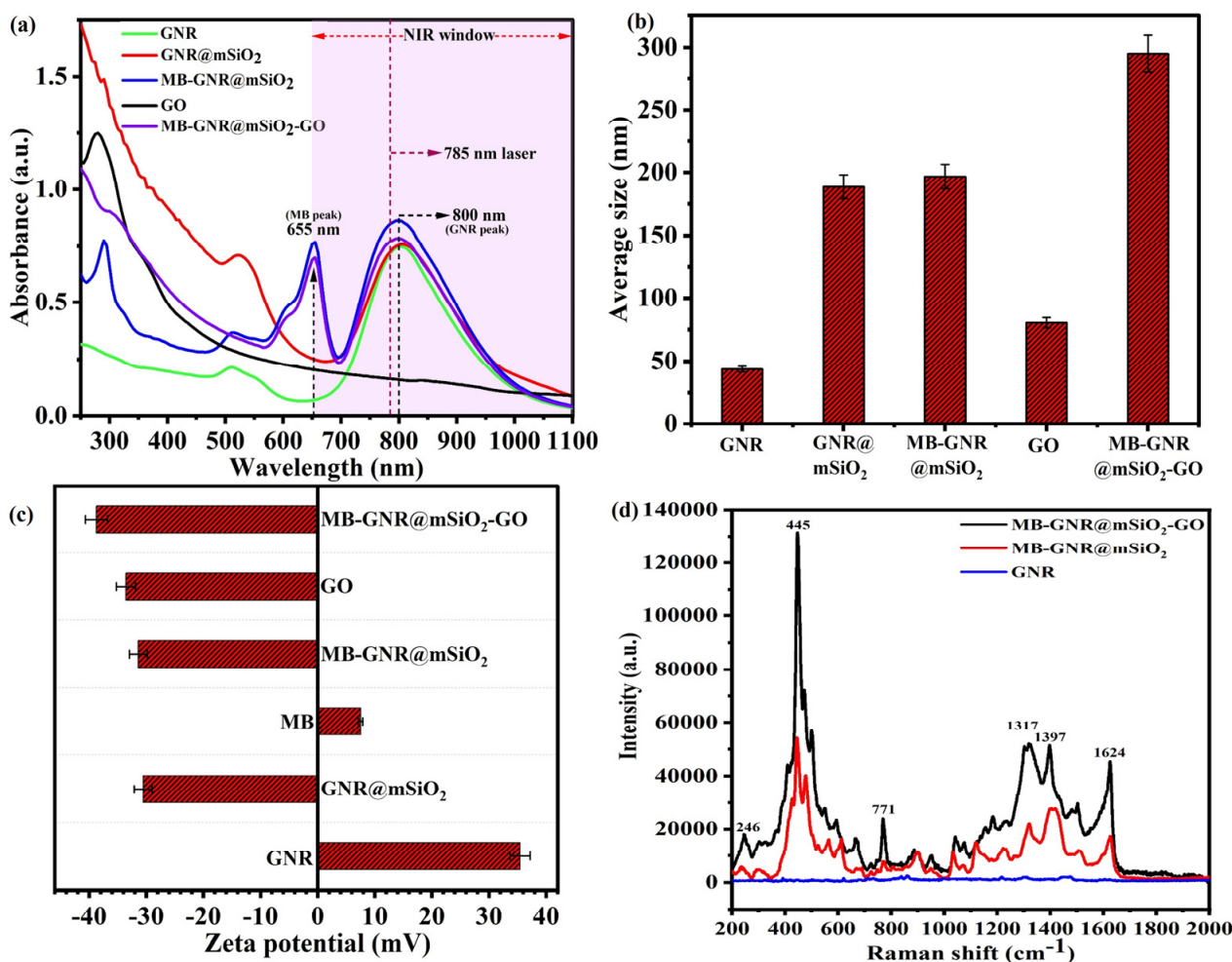


**Figure 3.** (a) UV-vis spectra of gold nanorods (GNRs), mesoporous silica-coated gold nanorods (GNR@mSiO<sub>2</sub>), methylene blue-loaded mesoporous silica-coated gold nanorods (MB-GNR@mSiO<sub>2</sub>), graphene oxide (GO), and methylene blue-loaded mesoporous silica-coated gold nanorods on graphene oxide (MB-GNR@mSiO<sub>2</sub>-GO). (b) Particle size distribution histograms of GNR, GNR@mSiO<sub>2</sub>, MB-GNR@mSiO<sub>2</sub>, GO, and MB-GNR@mSiO<sub>2</sub>-GO. (c) Zeta potential of GNR, GNR@mSiO<sub>2</sub>, MB-GNR@mSiO<sub>2</sub>, GO, and MB-GNR@mSiO<sub>2</sub>-GO. (d) MicroRaman spectra of GNR, MB-GNR@mSiO<sub>2</sub>, GO, and MB-GNR@mSiO<sub>2</sub>-GO solutions excited by a 785 nm laser (2 mW, spot area = 2–100 μm).

### 3.2. Measurement of Photothermal Performance

To further assess the photothermal efficacy of MB-GNR@mSiO<sub>2</sub>-GO, we examined the temperature variations of GNR, GNR@mSiO<sub>2</sub>, MB-GNR@mSiO<sub>2</sub>, GO, and MB-GNR@mSiO<sub>2</sub>-GO aqueous solutions (36 μg/mL) under a 785 nm laser irradiation at a power density of 0.8 W/cm<sup>2</sup> for 25 min (Figure 4a). The temperature variation of GNRs, GNR@mSiO<sub>2</sub>, MB-GNR@mSiO<sub>2</sub>, and GO aqueous solutions increased from 36.42 °C to 41.28 °C, which was insufficient to ablate the cancer cells. Meanwhile, the temperature variation of pure water only increased from 36.24 °C to 27.28 °C. In contrast, the temperature variation of the MB-GNR@mSiO<sub>2</sub>-GO aqueous solutions increased to 50.67 °C, which is sufficient for cancer therapy because cancer cells can be specifically eliminated at temperatures higher than hyperthermia (42–47 °C) [40]. Additionally, the Au concentration of MB-GNR@mSiO<sub>2</sub>-GO was calculated to be 36 μg Au/mL, and different volumes (0–200 μL of 36 μg/mL) of MB-GNR@mSiO<sub>2</sub>-GO aqueous solutions (1 mL) were added to a quartz cuvette and exposed to a 785 nm laser at 0.8 W/cm<sup>2</sup> for 25 min. The temperature variation of MB-GNR@mSiO<sub>2</sub>-GO (0, 50, 100, 150, and 200 μL of 36 μg/mL) aqueous solutions were exposed to a 785 nm

laser at  $0.8 \text{ W/cm}^2$  for 25 min, resulting in temperature values of  $37.4 \text{ }^\circ\text{C}$ ,  $45.79 \text{ }^\circ\text{C}$ ,  $48.72 \text{ }^\circ\text{C}$ ,  $49.71 \text{ }^\circ\text{C}$ , and  $52.12 \text{ }^\circ\text{C}$ , respectively (Figure 4b). The photothermal effect of the MB-GNR@mSiO<sub>2</sub>-GO (0, 50, 100, 150, and 200  $\mu\text{L}$  of  $36 \mu\text{g/mL}$ ) aqueous solutions was further examined using a FLIR thermal imaging camera (Figure 4c).

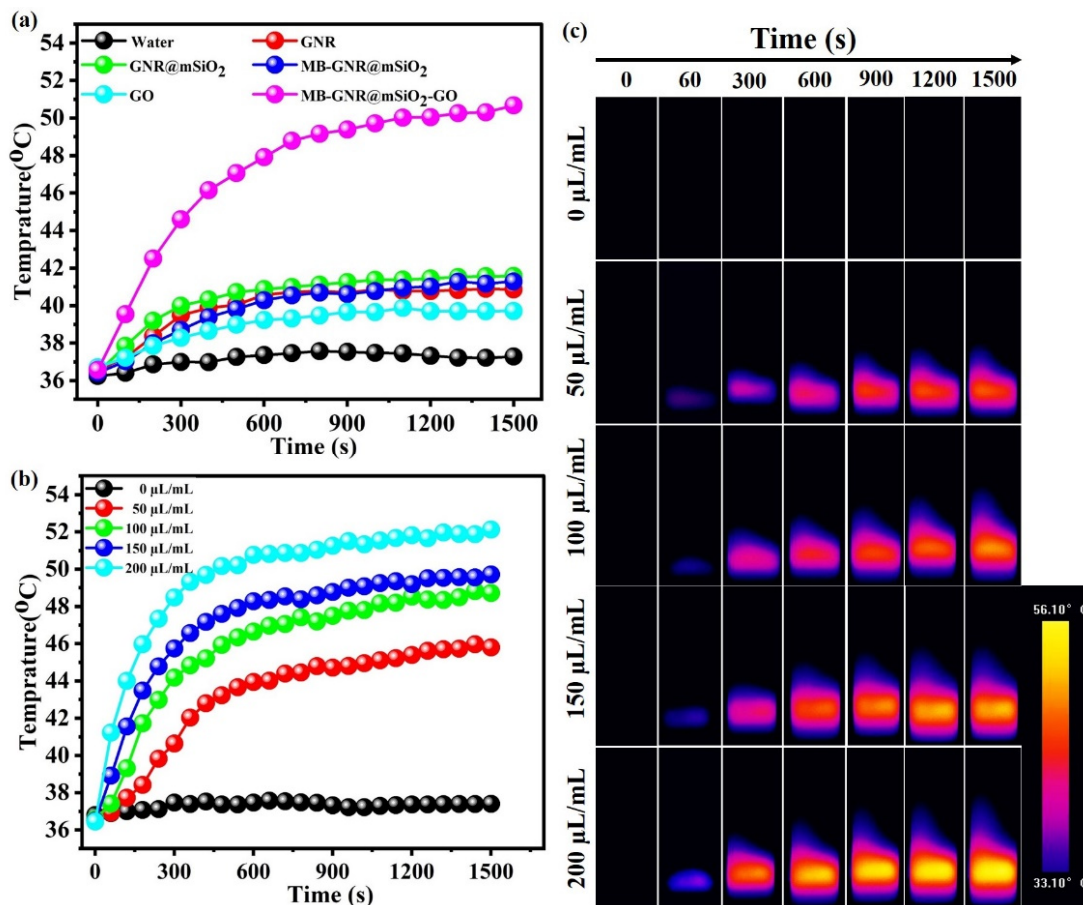


**Figure 4.** (a) The temperature variation curves of gold nanorods (GNRs), mesoporous silica-coated gold nanorods (GNR@mSiO<sub>2</sub>), methylene blue-loaded mesoporous silica-coated gold nanorods (MB-GNR@mSiO<sub>2</sub>), graphene oxide (GO), and methylene blue-loaded mesoporous silica-coated gold nanorods on graphene oxide (MB-GNR@mSiO<sub>2</sub>-GO) aqueous solutions ( $36 \mu\text{g/mL}$ ) under  $785 \text{ nm}$  laser irradiation at a power density of  $0.8 \text{ W/cm}^2$  for 25 min. (b) The temperature variation curves of MB-GNR@mSiO<sub>2</sub>-GO aqueous solutions with different volumes (0–200  $\mu\text{L}$  of  $36 \mu\text{g/mL}$ ) under  $785 \text{ nm}$  laser irradiation at a power density of  $0.8 \text{ W/cm}^2$  for 25 min. (c) IR thermal images of MB-GNR@mSiO<sub>2</sub>-GO aqueous solutions with different volumes (0–200  $\mu\text{L}$  of  $36 \mu\text{g/mL}$ ) under  $785 \text{ nm}$  laser irradiation at a power density of  $0.8 \text{ W/cm}^2$  for 25 min.

The photothermal conversion efficiency ( $\eta$ ) is a significant parameter used to quantify the ability of photothermal agents to convert light into heat [41]. To further demonstrate the photothermal conversion efficiency ( $\eta$ ) of the MB-GNR@mSiO<sub>2</sub>-GO aqueous solution, 1 mL of the MB-GNR@mSiO<sub>2</sub>-GO (200  $\mu\text{L}$  of  $36 \mu\text{g/mL}$ ) aqueous solution was exposed to a  $785 \text{ nm}$  laser at  $0.8 \text{ W/cm}^2$  for 25 min, turned off for 25 min, and then left to cool down to room temperature (Figure 5a). The value of  $t_s$  was 398.81 s. The photothermal conversion efficiency ( $\eta$ ) of MB-GNR@mSiO<sub>2</sub>-GO (200  $\mu\text{L/mL}$ ) was calculated to be 48.93% (Figure 5b), confirming that MB-GNR@mSiO<sub>2</sub>-GO has the best photothermal conversion capability, which was higher than that of commonly reported photothermal materials, such as GNRs (21%) [42], GO nanosheets (18%) [9], Fe<sub>3</sub>O<sub>4</sub>@CuS NPs (19.2%) [43], Cu<sub>2-x</sub>S nanocrystals (16.3%) [44], and Fe<sub>3</sub>O<sub>4</sub> nanoclusters (20.8%) [45]. More interestingly, the photothermal conversion efficiency of MB-GNR@mSiO<sub>2</sub>-GO was significantly higher (48.93%) than that

of either GNRs (21%) alone or GO nanosheets (18%) alone, which strongly supports the idea that the dual plasmonic photothermal agents have a synergistic plasmonic effect [9,46].

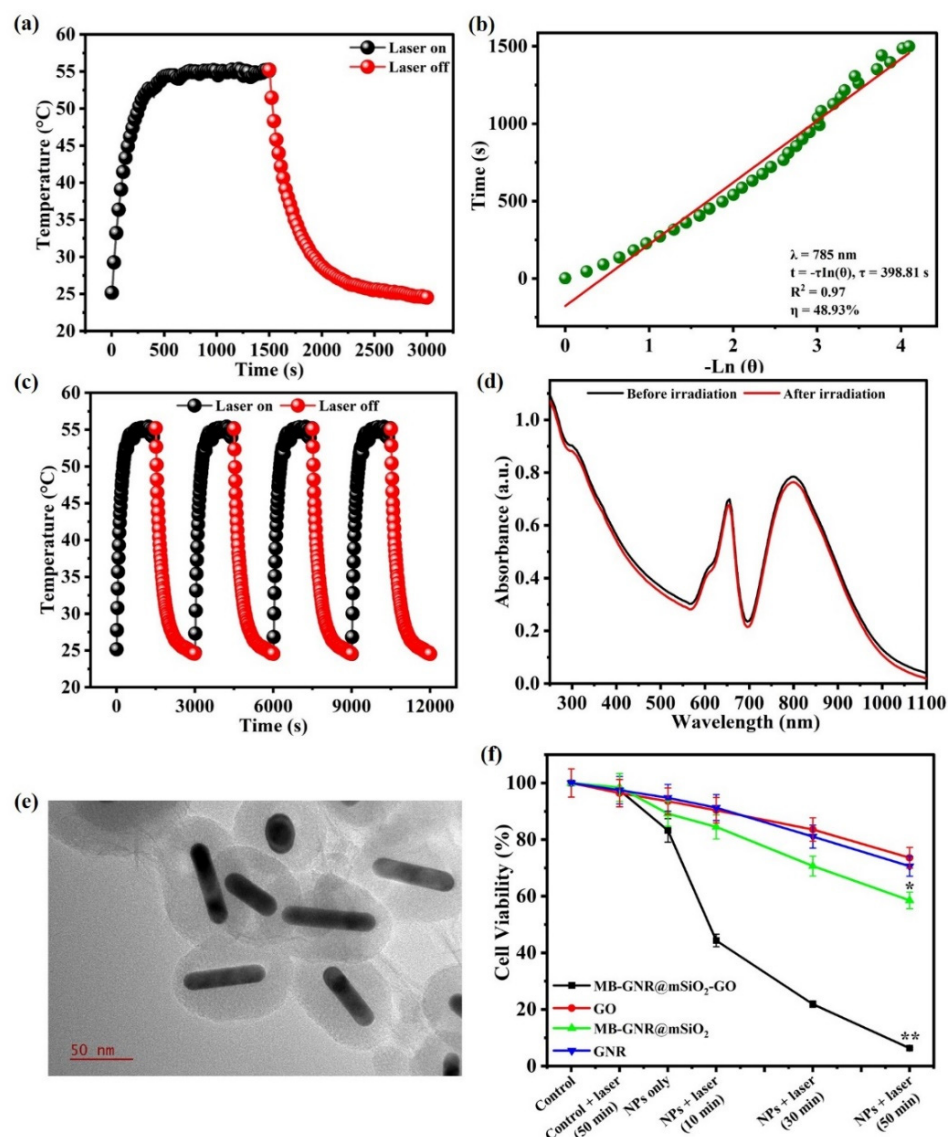


**Figure 5.** (a) The temperature variation curves of methylene blue-loaded mesoporous silica-coated gold nanorods on the graphene oxide (MB-GNR@mSiO<sub>2</sub>-GO) aqueous solution (200  $\mu$ L of 36  $\mu$ g/mL) under 785 nm laser irradiation at 0.8 W/cm<sup>2</sup> for 25 min, followed by natural cooling for 25 min. (b) The linear relationship of time data versus  $-\ln \theta$  obtained from the cooling period of the panel. (c) The temperature variation curves of the MB-GNR@mSiO<sub>2</sub>-GO aqueous solution (200  $\mu$ L of 36  $\mu$ g/mL) under four 785 nm laser on/off cycles (0.8 W/cm<sup>2</sup>). (d) UV-vis spectra of MB-GNR@mSiO<sub>2</sub>-GO before and after four cycles of laser irradiation. (e) Field emission transmission electron microscope (FETEM) image of MB-GNR@mSiO<sub>2</sub>-GO before and after four cycles of laser irradiation. (f) Viability of MDA-MB-231 cells treated with gold nanorods (GNRs), methylene blue-loaded mesoporous silica-coated gold nanorods (MB-GNR@mSiO<sub>2</sub>), graphene oxide (GO), and methylene blue-loaded mesoporous silica-coated gold nanorods on graphene oxide (MB-GNR@mSiO<sub>2</sub>-GO) (200  $\mu$ L of 36  $\mu$ g/mL) for 12 h of incubation with or without 785 nm laser irradiation at 0.8 W/cm<sup>2</sup> for various time points (0, 10, 30, and 50 min). Data were expressed as mean  $\pm$  S.D. ( $n = 3$ , \* significant  $p < 0.05$ , \*\* significant  $p < 0.01$ ).

It is widely known that GNR and GO have excellent heat-conducting properties, which are crucial for enhancing the photothermal stability of MB-GNR@mSiO<sub>2</sub>-GO (200  $\mu$ L of

36  $\mu\text{g}/\text{mL}$ ) [47]. To further evaluate the photothermal stability of MB-GNR@mSiO<sub>2</sub>-GO, the solution was placed in a quartz cuvette and then exposed to four cycles of laser on/off at 0.8 W/cm<sup>2</sup>. As shown in Figure 5c, no significant changes in the temperature variation were observed for MB-GNR@mSiO<sub>2</sub>-GO after four laser on/off cycles, indicating that MB-GNR@mSiO<sub>2</sub>-GO has good photothermal stability. Additionally, the UV-vis spectra of MB-GNR@mSiO<sub>2</sub>-GO were recorded after four cycles of laser irradiation (Figure 5d). The UV-vis spectra demonstrated that MB-GNR@mSiO<sub>2</sub>-GO exhibited no obvious changes in absorbance after four cycles of laser irradiation. MB-GNR@mSiO<sub>2</sub>-GO was also characterized using TEM, DLS, and ZP after four cycles of laser irradiation. The FETEM image of MB-GNR@mSiO<sub>2</sub>-GO also showed a uniform size and morphology after four cycles of laser irradiation (Figure 5e). The particle size of MB-GNR@mSiO<sub>2</sub>-GO after four cycles of laser irradiation was characterized by DLS as  $\sim 292.75 \pm 2.92$  nm. The ZP of MB-GNR@mSiO<sub>2</sub>-GO was  $-36.81 \pm 3.31$  mV. These results indicate that MB-GNR@mSiO<sub>2</sub>-GO has excellent photothermal stability after four cycles of laser irradiation [47].

### 3.3. In Vitro PTT/PDT Synergistic Effect

To evaluate the in vitro photothermal/photodynamic synergistic efficacy of GNR, MB-GNR@mSiO<sub>2</sub>, GO, and MB-GNR@mSiO<sub>2</sub>-GO, the BLO-11, and MDA-MB-231 cells were incubated with GNR, MB-GNR@mSiO<sub>2</sub>, GO, and MB-GNR@mSiO<sub>2</sub>-GO (200  $\mu\text{L}$  of 36  $\mu\text{g}/\text{mL}$ ) for 12 h and 48 h, and then were exposed to a 785 nm laser at 0.8 W/cm<sup>2</sup> for various time points (0, 10, 30, and 50 min). All cells were further incubated for 6 h, and their viability was determined by the MTT assay. As shown in Figure S2a,b, BLO-11 cells showed no obvious cytotoxicity without laser irradiation and the cell viability of BLO-11 cells with laser irradiation for 10, 30, and 50 min was above 80% when the high concentration of GNR, MB-GNR@mSiO<sub>2</sub>, and GO was 200  $\mu\text{L}$  of 36  $\mu\text{g}/\text{mL}$  for 12 h and 48 h, indicating that GNR, MB-GNR@mSiO<sub>2</sub>, and GO have excellent biocompatibility. The cell viability with laser irradiation for 10 and 30 min was above 80% at a higher concentration of MB-GNR@mSiO<sub>2</sub>-GO (200  $\mu\text{L}$  of 36  $\mu\text{g}/\text{mL}$ ) and the cell viability with laser irradiation for 50 min was more than 75% at a high concentration of MB-GNR@mSiO<sub>2</sub>-GO up to 200  $\mu\text{L}$  of 36  $\mu\text{g}/\text{mL}$ , suggesting very little cytotoxicity and good biocompatibility for the MB-GNR@mSiO<sub>2</sub>-GO. As shown in Figures 5f and S3, no noticeable cytotoxicity was observed in any of the treated groups for 12 h and 48 h of incubation without laser irradiation, suggesting that the as-prepared GNR, MB-GNR@mSiO<sub>2</sub>, GO, and MB-GNR@mSiO<sub>2</sub>-GO were highly biocompatible. However, upon irradiation, GNR, MB-GNR@mSiO<sub>2</sub>, and GO showed noticeable anticancer activity against MDA-MB-231 cells, which was 70.58%, 58.55%, and 73.57% for 12 h, and was 64.41%, 56.32%, and 71.42% for 48 h at the high concentration of GNR, MB-GNR@mSiO<sub>2</sub>, and GO up to 200  $\mu\text{L}$  of 36  $\mu\text{g}/\text{mL}$  and exposed to a 785 nm laser at 0.8 W/cm<sup>2</sup> for 50 min. The cells were treated with MB-GNR@mSiO<sub>2</sub>-GO (200  $\mu\text{L}$  of 36  $\mu\text{g}/\text{mL}$ ) for 12 h and 48 h and then were irradiated with a 785 nm laser at 0.8 W/cm<sup>2</sup> for 50 min, which showed significantly reduced cell viability (6.32% and 4.46%), demonstrating the possibility that laser irradiation could boost the cytotoxic effects of MB-GNR@mSiO<sub>2</sub>-GO [34]. As shown in Figures 5f and S3, no significant difference was observed after 12 h and 48 h incubation with GNR, MB-GNR@mSiO<sub>2</sub>, GO, and MB-GNR@mSiO<sub>2</sub>-GO (200  $\mu\text{L}$  of 36  $\mu\text{g}/\text{mL}$ ) with or without laser irradiation, confirming that all the materials have very little toxicity to cells without laser irradiation; in addition, all the materials with laser irradiation for 50 min showed significant cytotoxicity to MDA-MB-231 cells because these materials have excellent photothermal conversion properties.

The photothermal effects of GNR, MB-GNR@mSiO<sub>2</sub>, and MB-GNR@mSiO<sub>2</sub>-GO on MDA-MB-231 cells were further confirmed using calcein-AM and PI co-staining to visually differentiate live (green) and dead (red) cells. As shown in Figure 6, there were no cellular deaths in the control only, control with laser irradiation, GNR only, GNR with laser irradiation, MB-GNR@mSiO<sub>2</sub> only, MB-GNR@mSiO<sub>2</sub> with laser irradiation, and MB-GNR@mSiO<sub>2</sub>-GO only groups because all of the cells showed green fluorescence and negligible cell deaths in these groups. In contrast, MB-GNR@mSiO<sub>2</sub>-GO with laser irradiation

tion showed strong red fluorescence, and a large red area was observed, suggesting that MB-GNR@mSiO<sub>2</sub>-GO with laser irradiation induced complete cellular destruction [48].

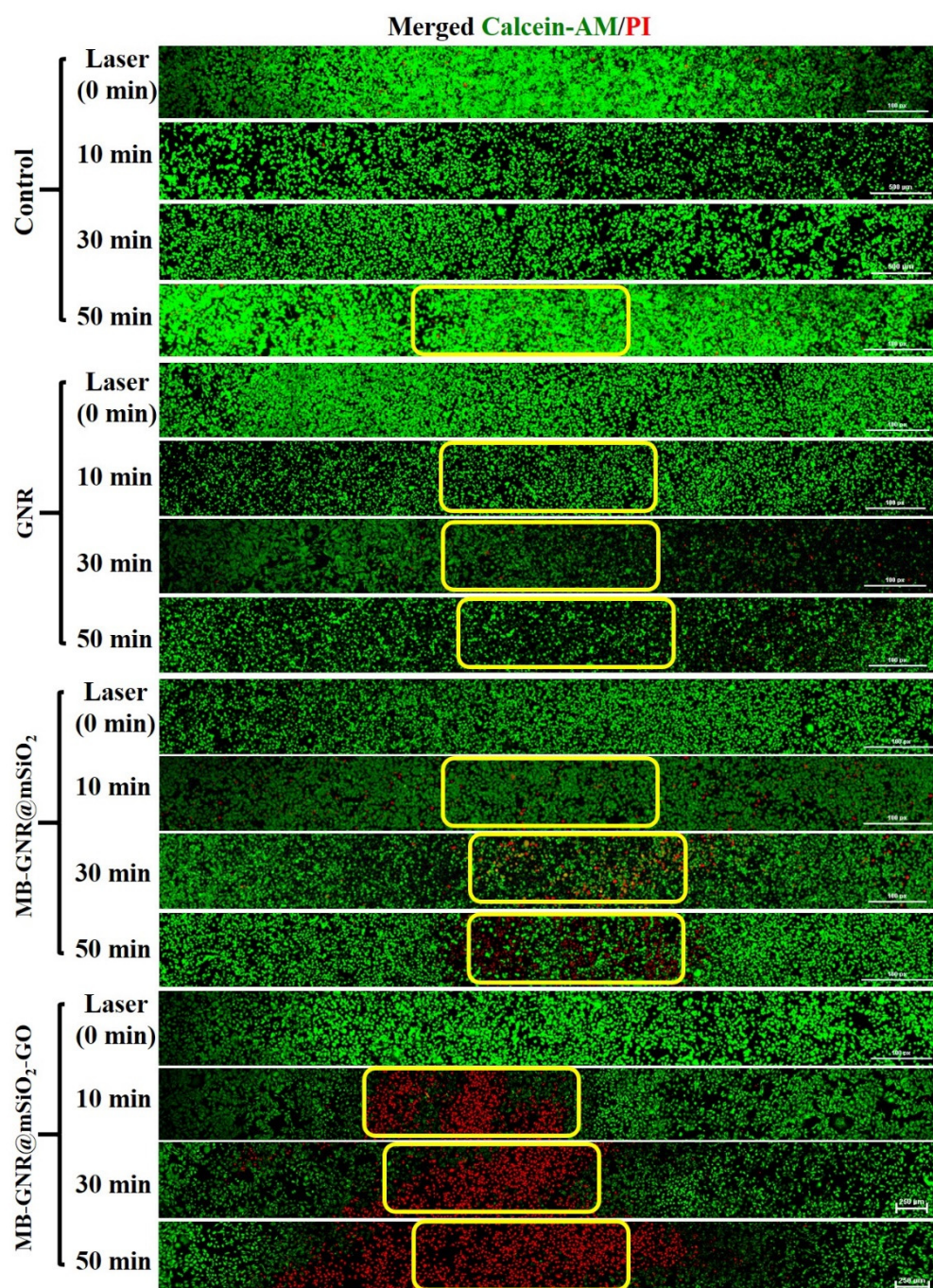


**Figure 6.** Merged confocal fluorescence images of MDA-MB-231 cells treated with gold nanorods (GNRs), methylene blue-loaded mesoporous silica-coated gold nanorods (MB-GNR@mSiO<sub>2</sub>), and methylene blue-loaded mesoporous silica-coated gold nanorods on graphene oxide (MB-GNR@mSiO<sub>2</sub>-GO) (200  $\mu$ L of 36  $\mu$ g/mL) for 12 h with or without 785 nm laser irradiation at 0.8 W/cm<sup>2</sup> for various time points (0, 10, 30, and 50 min). The cells were stained using calcein-AM (live: green) and PI (dead: red) (20 $\times$  magnification). The yellow color indicates the laser spot area.

To evaluate the photodynamic effect of GNR, MB-GNR@mSiO<sub>2</sub>, and MB-GNR@mSiO<sub>2</sub>-GO on intracellular ROS generation, DCHF-DA was used as a fluorescent dye to monitor changes in the intracellular ROS levels. As shown in Figure 7, no strong green signal

was detected in the control only, control with laser irradiation, GNR only, GNR with laser irradiation, MB-GNR@mSiO<sub>2</sub> only, MB-GNR@mSiO<sub>2</sub> with laser irradiation, and MB-GNR@mSiO<sub>2</sub>-GO only groups, which did not damage the cancer cells. In contrast, MB-GNR@mSiO<sub>2</sub>-GO produced strong green fluorescence after 785 nm laser irradiation for 50 min, which could damage biomolecules and cellular organs such as the mitochondria and nucleus, implying the generation of ROS [49].

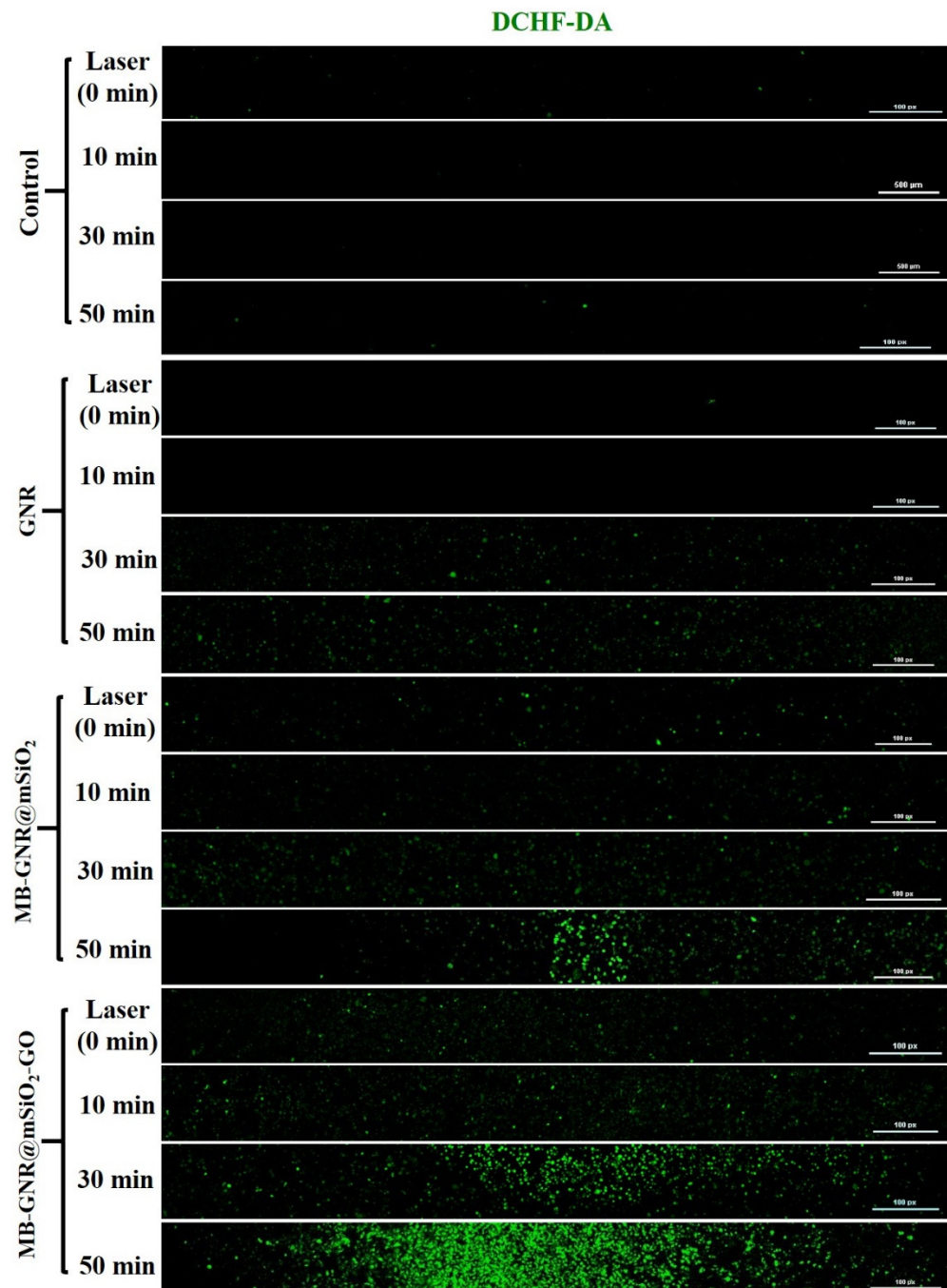


**Figure 7.** DCHF-DA staining confocal fluorescence images of MDA-MB-231 cells treated with gold nanorods (GNRs), methylene blue-loaded mesoporous silica-coated gold nanorods (MB-GNR@mSiO<sub>2</sub>), and methylene blue-loaded mesoporous silica-coated gold nanorods on graphene oxide (MB-GNR@mSiO<sub>2</sub>-GO) (200 µL of 36 µg/mL) with or without 785 nm laser irradiation at 0.8 W/cm<sup>2</sup> for various time points (0, 10, 30, and 50 min) (20× magnification).

### 3.4. Surface-Enhanced Raman Scattering (SERS) Imaging

Surface-enhanced Raman scattering (SERS) imaging is a technique for boosting the Raman signals of molecules using nanomaterials, such as metal colloids [50]. SERS has drawn much interest in the field of biological research and has emerged as an effective imaging method for early cancer detection [51]. The bright-field images and SERS spectra of the GNR (control), MB-GNR@mSiO<sub>2</sub>, and MB-GNR@mSiO<sub>2</sub>-GO-treated MDA-MB-231 cells under an excitation laser of 785 nm are shown in Figure 8a–c. Strong SERS peaks were observed for MB-GNR@mSiO<sub>2</sub> and MB-GNR@mSiO<sub>2</sub>-GO, whereas no SERS peaks were observed for the control. The SERS peaks of MB-GNR@mSiO<sub>2</sub> and MB-GNR@mSiO<sub>2</sub>-GO were clearly observed at 445 cm<sup>-1</sup>, 1397 cm<sup>-1</sup>, and 1624 cm<sup>-1</sup>, which were assigned to the C–N–C skeletal deformation mode ( $\delta(\text{C–N–C})$ ),  $\nu_{\text{sym}}(\text{C–N})$ , and  $\nu(\text{C–C})_{\text{ring}}$  modes, indicating that the SERS peaks of MB-GNR@mSiO<sub>2</sub>-GO were sufficient to detect cancer at an early stage.

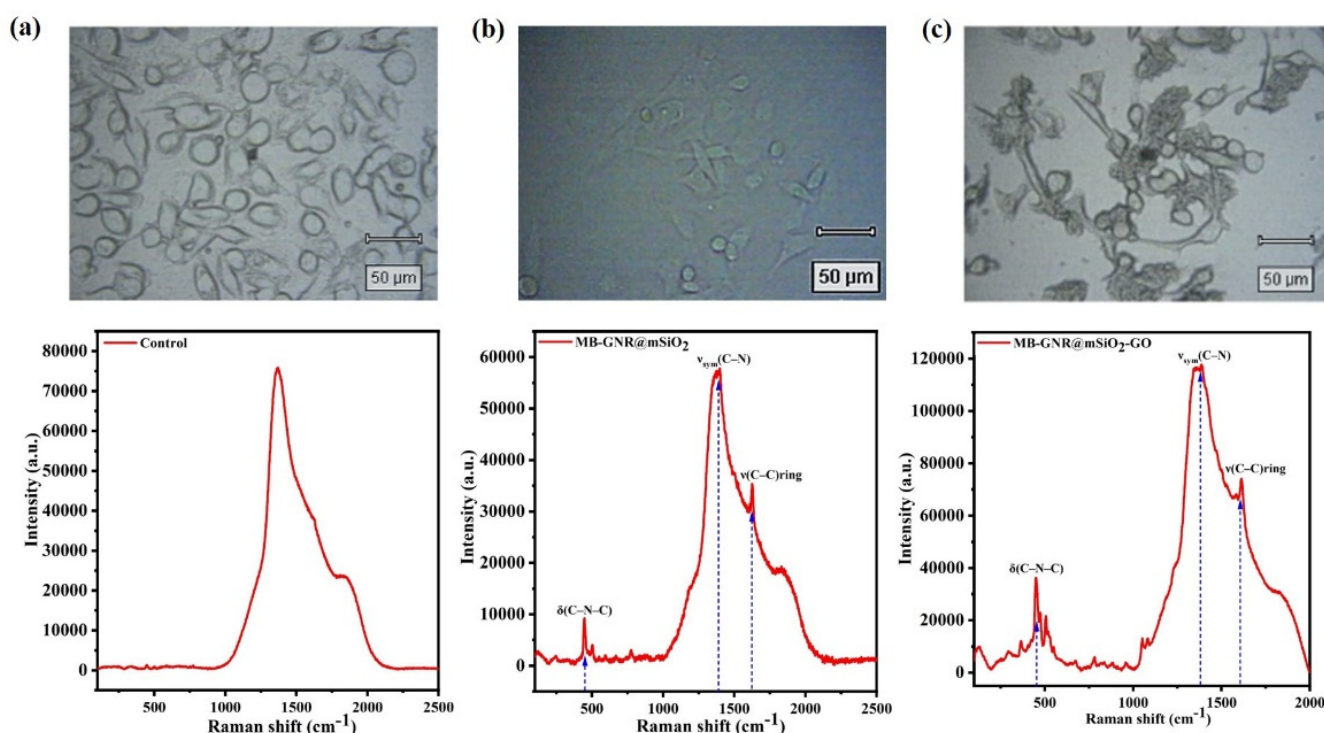


**Figure 8.** Bright-field images and micro-Raman spectra of MDA-MB-231 cells treated with control (a), methylene blue-loaded mesoporous silica-coated gold nanorods (MB-GNR@mSiO<sub>2</sub>) (b), and methylene blue-loaded mesoporous silica-coated gold nanorods on graphene oxide (MB-GNR@mSiO<sub>2</sub>-GO) (c). The bright-field images indicate the laser-activated area ( $\lambda = 785$  nm, 2 mW, spot area = 2–100  $\mu\text{m}$ ).

### 4. Conclusions

In summary, we successfully designed and developed multifunctional MB-GNR@mSiO<sub>2</sub>-GO as a new phototheranostic agent for intracellular SERS imaging-guided synergistic PTT/PDT of cancer. MB-GNR@mSiO<sub>2</sub>-GO showed strong SPR absorption in the NIR region, high MB loading capability, high photothermal conversion efficiency (48.93%), superior photothermal stability, and a strong SERS effect. The *in vitro* cytotoxicity of MB-GNR@mSiO<sub>2</sub>-GO had excellent biocompatibility in the absence of laser irradiation. Most intriguingly, the strong SERS effect of MB-GNR@mSiO<sub>2</sub>-GO permits accurate cancer cell detection by SERS imaging, and the cells treated with MB-GNR@mSiO<sub>2</sub>-GO and laser irradiation led to significant cell death, confirming that MB-GNR@mSiO<sub>2</sub>-GO has a strong SERS effect and superior photothermal efficiency under laser irradiation. The *in vitro* photodynamic effect of MB-GNR@mSiO<sub>2</sub>-GO showed enhanced cell apoptosis under laser irradiation, which could damage the mitochondria and nucleus, indicat-

ing that MB-GNR@mSiO<sub>2</sub>-GO has excellent ROS generation capability with the help of 785 nm laser irradiation. We believe that this multifunctional MB-GNR@mSiO<sub>2</sub>-GO has great potential for further clinical applications in the diagnosis and therapy of cancer.

**Supplementary Materials:** The following supporting information can be downloaded at: <https://www.mdpi.com/article/10.3390/pharmaceutics14102242/s1>, Figure S1: FETEM images of methylene blue-loaded mesoporous silica-coated gold nanorods on graphene oxide (MB-GNR@mSiO<sub>2</sub>-GO); Figure S2: Viability of BLO-11 cells treated with gold nanorod (GNR), methylene blue-loaded mesoporous silica-coated gold nanorod (MB-GNR@mSiO<sub>2</sub>), graphene oxide (GO), and methylene blue-loaded mesoporous silica-coated gold nanorods on graphene oxide (MB-GNR@mSiO<sub>2</sub>-GO) (200 µL/mL) for 12 h (a) and 48 h (b) with or without 785 nm laser irradiation at 0.8 W/cm<sup>2</sup> for various time points (0, 10, 30, and 50 min). Data were expressed as mean ± S.D. (*n* = 3); Figure S3: Viability of MDA-MB-231 cells treated with gold nanorod (GNR), methylene blue-loaded mesoporous silica-coated gold nanorod (MB-GNR@mSiO<sub>2</sub>), graphene oxide (GO), and methylene blue-loaded mesoporous silica-coated gold nanorods on graphene oxide (MB-GNR@mSiO<sub>2</sub>-GO) (200 µL/mL) for 48 h with or without 785 nm laser irradiation at 0.8 W/cm<sup>2</sup> for various time points (0, 10, 30, and 50 min). Data were expressed as mean ± S.D. (*n* = 3, \* significant *p* < 0.05, \*\* significant *p* < 0.01).

**Author Contributions:** The manuscript was written through the contributions of all authors. Conceptualization, S.-H.S. and A.J.; investigation, A.J. and H.-W.H.; formal analysis, S.-H.S. and H.-W.H.; data curation, S.-H.S., writing—original draft preparation, P.M.; data curation, E.-S.J.; funding acquisition, E.-S.J. All authors have read and agreed to the published version of the manuscript.

**Funding:** E.-S.J. is especially grateful for the research grant from the Korean Ministry of Education, Science & Technology (2016R1D1A3B0201175615) and the Grand Information Technology Research Center Program (IITP-2022-2020-0-01612) through the Institute of Information & Communications Technology Planning & Evaluation (IITP) funded by the Ministry of Science and ICT (MSIT), Korea. This research was supported by the Basic Science Research Program through the National Research Foundation of Korea (NRF), funded by the Ministry of Education (NRF-2022R111A1A01068693).

**Institutional Review Board Statement:** Not applicable.

**Informed Consent Statement:** Not applicable.

**Data Availability Statement:** Not applicable.

**Conflicts of Interest:** The authors declare no conflict of interest.

## References

1. Shao, W.; Yang, C.; Li, F.; Wu, J.; Wang, N.; Ding, Q.; Gao, J.; Ling, D. Molecular design of conjugated small molecule nanoparticles for synergistically enhanced PTT/PDT. *Nano-Micro Lett.* **2020**, *12*, 147. [[CrossRef](#)] [[PubMed](#)]
2. Ferrari, M. Cancer nanotechnology: Opportunities and challenges. *Nat. Rev. Cancer* **2005**, *5*, 161–171. [[CrossRef](#)] [[PubMed](#)]
3. Wu, C.; Li, D.; Wang, L.; Guan, X.; Tian, Y.; Yang, H.; Li, S.; Liu, Y. Single wavelength light-mediated, synergistic bimodal cancer photoablation and amplified photothermal performance by graphene/gold nanostar/photosensitizer theranostics. *Acta Biomater.* **2017**, *53*, 631–642. [[CrossRef](#)] [[PubMed](#)]
4. Li, M.; Xu, J.; Romero-Gonzalez, M.; Banwart, S.A.; Huang, W.E. Single cell Raman spectroscopy for cell sorting and imaging. *Curr. Opin. Biotechnol.* **2012**, *23*, 56–63. [[CrossRef](#)]
5. Park, H.; Lee, S.; Chen, L.; Lee, E.K.; Shin, S.Y.; Lee, Y.H.; Son, S.W.; Oh, C.H.; Song, J.M.; Kang, S.H. SERS imaging of HER2-overexpressed MCF7 cells using antibody-conjugated gold nanorods. *Phys. Chem. Chem. Phys.* **2009**, *11*, 7444–7449. [[CrossRef](#)]
6. Cheng, L.; Wang, C.; Feng, L.; Yang, K.; Liu, Z. Functional nanomaterials for phototherapies of cancer. *Chem. Rev.* **2014**, *114*, 10869–10939. [[CrossRef](#)]
7. Manivasagan, P.; Bharathiraja, S.; Moorthy, M.S.; Oh, Y.-O.; Seo, H.; Oh, J. Marine biopolymer-based nanomaterials as a novel platform for theranostic applications. *Polym. Rev.* **2017**, *57*, 631–667. [[CrossRef](#)]
8. Deng, K.; Liu, D.; Wang, Z.; Zhou, Z.; Chen, Q.; Luo, J.; Zhang, Y.; Hou, Z.; Lin, J. Surface-Functionalized NdVO<sub>4</sub>: Gd<sup>3+</sup> Nanoplates as Active Agents for Near-Infrared-Light-Triggered and Multimodal-Imaging-Guided Photothermal Therapy. *Pharmaceutics* **2022**, *14*, 1217. [[CrossRef](#)] [[PubMed](#)]
9. Younis, M.R.; An, R.B.; Yin, Y.-C.; Wang, S.; Ye, D.; Xia, X.-H. Plasmonic nanohybrid with high photothermal conversion efficiency for simultaneously effective antibacterial/anticancer photothermal therapy. *ACS Appl. Bio Mater.* **2019**, *2*, 3942–3953. [[CrossRef](#)] [[PubMed](#)]

10. Li, J.; Rao, J.; Pu, K. Recent progress on semiconducting polymer nanoparticles for molecular imaging and cancer phototherapy. *Biomaterials* **2018**, *155*, 217–235. [[CrossRef](#)] [[PubMed](#)]
11. Gong, H.; Peng, R.; Liu, Z. Carbon nanotubes for biomedical imaging: The recent advances. *Adv. Drug Deliv. Rev.* **2013**, *65*, 1951–1963. [[CrossRef](#)] [[PubMed](#)]
12. Li, Y.; Lu, W.; Huang, Q.; Li, C.; Chen, W. Copper sulfide nanoparticles for photothermal ablation of tumor cells. *Nanomedicine* **2010**, *5*, 1161–1171. [[CrossRef](#)] [[PubMed](#)]
13. Narayanan, N.; Kim, J.H.; Santhakumar, H.; Joseph, M.M.; Karunakaran, V.; Shamjith, S.; Saranya, G.; Sujai, P.T.; Jayasree, R.S.; Barman, I. Nanotheranostic Probe Built on Methylene Blue Loaded Cucurbituril [8] and Gold Nanorod: Targeted Phototherapy in Combination with SERS Imaging on Breast Cancer Cells. *J. Phys. Chem. B* **2021**, *125*, 13415–13424. [[CrossRef](#)] [[PubMed](#)]
14. Huang, X.; Neretina, S.; El-Sayed, M.A. Gold nanorods: From synthesis and properties to biological and biomedical applications. *Adv. Mater.* **2009**, *21*, 4880–4910. [[CrossRef](#)]
15. Nikoobakht, B.; El-Sayed, M.A. Preparation and growth mechanism of gold nanorods (NRs) using seed-mediated growth method. *Chem. Mater.* **2003**, *15*, 1957–1962. [[CrossRef](#)]
16. Kim, H.J.; Wang, W.; Bu, W.; Hossen, M.M.; Londono-Calderon, A.; Hillier, A.C.; Prozorov, T.; Mallapragada, S.; Vaknin, D. Salt mediated self-assembly of poly (ethylene glycol)-functionalized gold nanorods. *Sci. Rep.* **2019**, *9*, 20349. [[CrossRef](#)]
17. Terentyuk, G.; Panfilova, G.; Khanadeev, V.; Chumakov, D.; Genina, E.; Bashkatov, A.; Tuchin, V.; Bucharskaya, A.; Maslyakova, G.; Khlebtsov, N. Gold nanorods with a hematoporphyrin-loaded silica shell for dual-modality photodynamic and photothermal treatment of tumors in vivo. *Nano Res.* **2014**, *7*, 325–337. [[CrossRef](#)]
18. Tsai, M.-F.; Chang, S.-H.G.; Cheng, F.-Y.; Shanmugam, V.; Cheng, Y.-S.; Su, C.-H.; Yeh, C.-S. Au nanorod design as light-absorber in the first and second biological near-infrared windows for in vivo photothermal therapy. *ACS Nano* **2013**, *7*, 5330–5342. [[CrossRef](#)]
19. Stöber, W.; Fink, A.; Bohn, E. Controlled growth of monodisperse silica spheres in the micron size range. *J. Colloid Interface Sci.* **1968**, *26*, 62–69. [[CrossRef](#)]
20. Khatiri, R.; Reyhani, A.; Mortazavi, S.; Hossainipour, M. Immobilization of serum albumin on the synthesized three layers core-shell structures of super-paramagnetic iron oxide nanoparticles. *J. Ind. Eng. Chem.* **2013**, *19*, 1642–1647. [[CrossRef](#)]
21. Huang, P.; Zeng, B.; Mai, Z.; Deng, J.; Fang, Y.; Huang, W.; Zhang, H.; Yuan, J.; Wei, Y.; Zhou, W. Novel drug delivery nanosystems based on out-inside bifunctionalized mesoporous silica yolk-shell magnetic nanostars used as nanocarriers for curcumin. *J. Mater. Chem. B* **2016**, *4*, 46–56. [[CrossRef](#)]
22. Zhang, Z.; Wang, L.; Wang, J.; Jiang, X.; Li, X.; Hu, Z.; Ji, Y.; Wu, X.; Chen, C. Mesoporous silica-coated gold nanorods as a light-mediated multifunctional theranostic platform for cancer treatment. *Adv. Mater.* **2012**, *24*, 1418–1423. [[CrossRef](#)]
23. Tardivo, J.P.; Del Giglio, A.; De Oliveira, C.S.; Gabrielli, D.S.; Junqueira, H.C.; Tada, D.B.; Severino, D.; de Fátima Turchiello, R.; Baptista, M.S. Methylene blue in photodynamic therapy: From basic mechanisms to clinical applications. *Photodiagn. Photodyn. Ther.* **2005**, *2*, 175–191. [[CrossRef](#)]
24. Kohle, F.F.; Li, S.; Turker, M.Z.; Wiesner, U.B. Ultrasmall PEGylated and targeted core-shell silica nanoparticles carrying methylene blue photosensitizer. *ACS Biomater. Sci. Eng.* **2019**, *6*, 256–264. [[CrossRef](#)]
25. Seo, S.-H.; Kim, B.-M.; Joe, A.; Han, H.-W.; Chen, X.; Cheng, Z.; Jang, E.-S. NIR-light-induced surface-enhanced Raman scattering for detection and photothermal/photodynamic therapy of cancer cells using methylene blue-embedded gold nanorod@ SiO<sub>2</sub> nanocomposites. *Biomaterials* **2014**, *35*, 3309–3318. [[CrossRef](#)]
26. Zhang, Z.; Shi, J.; Song, Z.; Zhu, X.; Zhu, Y.; Cao, S. A synergistically enhanced photothermal transition effect from mesoporous silica nanoparticles with gold nanorods wrapped in reduced graphene oxide. *J. Mater. Sci.* **2018**, *53*, 1810–1823. [[CrossRef](#)]
27. Gorelikov, I.; Matsuura, N. Single-step coating of mesoporous silica on cetyltrimethyl ammonium bromide-capped nanoparticles. *Nano Lett.* **2008**, *8*, 369–373. [[CrossRef](#)]
28. Han, H.-W.; Joe, A.; Jang, E.-S. Reduced cytotoxicity of CTAB-templated silica layer on gold nanorod using fluorescence dyes and its application in cancer theranostics. *J. Ind. Eng. Chem.* **2021**, *96*, 202–212. [[CrossRef](#)]
29. Hummers, W.S., Jr.; Offeman, R.E. Preparation of graphitic oxide. *J. Am. Chem. Soc.* **1958**, *80*, 1339. [[CrossRef](#)]
30. Roper, D.K.; Ahn, W.; Hoepfner, M. Microscale heat transfer transduced by surface plasmon resonant gold nanoparticles. *J. Phys. Chem. C* **2007**, *111*, 3636–3641. [[CrossRef](#)]
31. Liu, X.; Li, B.; Fu, F.; Xu, K.; Zou, R.; Wang, Q.; Zhang, B.; Chen, Z.; Hu, J. Facile synthesis of biocompatible cysteine-coated CuS nanoparticles with high photothermal conversion efficiency for cancer therapy. *Dalton Trans.* **2014**, *43*, 11709–11715. [[CrossRef](#)] [[PubMed](#)]
32. Yang, Y.-H.; Liu, C.-H.; Liang, Y.-H.; Lin, F.-H.; Wu, K.C.-W. Hollow mesoporous hydroxyapatite nanoparticles (hmHANPs) with enhanced drug loading and pH-responsive release properties for intracellular drug delivery. *J. Mater. Chem. B* **2013**, *1*, 2447–2450. [[CrossRef](#)] [[PubMed](#)]
33. Xia, H.-X.; Yang, X.-Q.; Song, J.-T.; Chen, J.; Zhang, M.-Z.; Yan, D.-M.; Zhang, L.; Qin, M.-Y.; Bai, L.-Y.; Zhao, Y.-D. Folic acid-conjugated silica-coated gold nanorods and quantum dots for dual-modality CT and fluorescence imaging and photothermal therapy. *J. Mater. Chem. B* **2014**, *2*, 1945–1953. [[CrossRef](#)]
34. Manivasagan, P.; Jun, S.W.; Truong, N.T.P.; Hoang, G.; Mondal, S.; Moorthy, M.S.; Kim, H.; Phan, T.T.V.; Doan, V.H.M.; Kim, C.-S. A multifunctional near-infrared laser-triggered drug delivery system using folic acid conjugated chitosan oligosaccharide encapsulated gold nanorods for targeted chemo-photothermal therapy. *J. Mater. Chem. B* **2019**, *7*, 3811–3825. [[CrossRef](#)]

35. Liu, X.; Liu, L.; Hu, X.; Zhou, S.; Ankri, R.; Fixler, D.; Xie, Z. Multimodal bioimaging based on gold nanorod and carbon dot nanohybrids as a novel tool for atherosclerosis detection. *Nano Res.* **2018**, *11*, 1262–1273. [[CrossRef](#)]
36. Planas, O.; Bresolí-Obach, R.; Nos, J.; Gallavardin, T.; Ruiz-González, R.; Agut, M.; Nonell, S. Synthesis, photophysical characterization, and photoinduced antibacterial activity of methylene blue-loaded amino- and mannose-targeted mesoporous silica nanoparticles. *Molecules* **2015**, *20*, 6284–6298. [[CrossRef](#)] [[PubMed](#)]
37. Xing, C.; Jing, G.; Liang, X.; Qiu, M.; Li, Z.; Cao, R.; Li, X.; Fan, D.; Zhang, H. Graphene oxide/black phosphorus nanoflake aerogels with robust thermo-stability and significantly enhanced photothermal properties in air. *Nanoscale* **2017**, *9*, 8096–8101. [[CrossRef](#)]
38. Fang, S.; Lin, J.; Li, C.; Huang, P.; Hou, W.; Zhang, C.; Liu, J.; Huang, S.; Luo, Y.; Fan, W. Dual-stimuli responsive nanotheranostics for multimodal imaging guided trimodal synergistic therapy. *Small* **2017**, *13*, 1602580. [[CrossRef](#)] [[PubMed](#)]
39. Shim, K.D.; Jang, E.S. SERS Signal Enhancement of Methylene Blue-embedded Agglomerated Gold Nanorod@ SiO<sub>2</sub> Core@ Shell Composites. *Bull. Korean Chem. Soc.* **2018**, *39*, 936–940. [[CrossRef](#)]
40. Manivasagan, P.; Jun, S.W.; Hoang, G.; Mondal, S.; Kim, H.; Doan, V.H.M.; Kim, J.; Kim, C.-S.; Oh, J. Anti-EGFR antibody conjugated thiol chitosan-layered gold nanoshells for dual-modal imaging-guided cancer combination therapy. *J. Control. Release* **2019**, *311*, 26–42. [[CrossRef](#)]
41. Yu, X.; Yang, K.; Chen, X.; Li, W. Black hollow silicon oxide nanoparticles as highly efficient photothermal agents in the second near-infrared window for in vivo cancer therapy. *Biomaterials* **2017**, *143*, 120–129. [[CrossRef](#)] [[PubMed](#)]
42. Hessel, C.M.; Pattani, V.P.; Rasch, M.; Panthani, M.G.; Koo, B.; Tunnell, J.W.; Korgel, B.A. Copper selenide nanocrystals for photothermal therapy. *Nano Lett.* **2011**, *11*, 2560–2566. [[CrossRef](#)]
43. Wu, Z.C.; Li, W.P.; Luo, C.H.; Su, C.H.; Yeh, C.S. Rattle-Type Fe<sub>3</sub>O<sub>4</sub>@ CuS Developed to Conduct Magnetically Guided Photoinduced Hyperthermia at First and Second NIR Biological Windows. *Adv. Funct. Mater.* **2015**, *25*, 6527–6537. [[CrossRef](#)]
44. Wang, S.; Riedinger, A.; Li, H.; Fu, C.; Liu, H.; Li, L.; Liu, T.; Tan, L.; Barthel, M.J.; Pugliese, G. Plasmonic copper sulfide nanocrystals exhibiting near-infrared photothermal and photodynamic therapeutic effects. *ACS Nano* **2015**, *9*, 1788–1800. [[CrossRef](#)] [[PubMed](#)]
45. Huang, C.-C.; Chang, P.-Y.; Liu, C.-L.; Xu, J.-P.; Wu, S.-P.; Kuo, W.-C. New insight on optical and magnetic Fe<sub>3</sub>O<sub>4</sub> nanoclusters promising for near infrared theranostic applications. *Nanoscale* **2015**, *7*, 12689–12697. [[CrossRef](#)] [[PubMed](#)]
46. Manivasagan, P.; Joe, A.; Han, H.-W.; Thambi, T.; Selvaraj, M.; Chidambaram, K.; Kim, J.; Jang, E.-S. Recent advances in multifunctional nanomaterials for photothermal-enhanced Fenton-based chemodynamic tumor therapy. *Mater. Today Bio* **2022**, *13*, 100197. [[CrossRef](#)] [[PubMed](#)]
47. Qi, Z.; Shi, J.; Zhang, Z.; Cao, Y.; Li, J.; Cao, S. PEGylated graphene oxide-capped gold nanorods/silica nanoparticles as multifunctional drug delivery platform with enhanced near-infrared responsiveness. *Mater. Sci. Eng. C* **2019**, *104*, 109889. [[CrossRef](#)] [[PubMed](#)]
48. Wang, H.; Zhang, M.; Zhang, L.; Li, S.; Li, L.; Li, X.; Yu, M.; Mou, Z.; Wang, T.; Wang, C. Near-infrared light and pH-responsive Au@ carbon/calcium phosphate nanoparticles for imaging and chemo-photothermal cancer therapy of cancer cells. *Dalton Trans.* **2017**, *46*, 14746–14751. [[CrossRef](#)] [[PubMed](#)]
49. Bharathiraja, S.; Moorthy, M.S.; Manivasagan, P.; Seo, H.; Lee, K.D.; Oh, J. Chlorin e6 conjugated silica nanoparticles for targeted and effective photodynamic therapy. *Photodiagn. Photodyn. Ther.* **2017**, *19*, 212–220. [[CrossRef](#)] [[PubMed](#)]
50. Moisoiu, V.; Socaciu, A.; Stefanu, A.; Iancu, S.D.; Boros, I.; Alecsa, C.D.; Rachieriu, C.; Chiorean, A.R.; Eniu, D.; Leopold, N. Breast cancer diagnosis by surface-enhanced Raman scattering (SERS) of urine. *Appl. Sci.* **2019**, *9*, 806. [[CrossRef](#)]
51. Sun, C.; Gao, M.; Zhang, X. Surface-enhanced Raman scattering (SERS) imaging-guided real-time photothermal ablation of target cancer cells using polydopamine-encapsulated gold nanorods as multifunctional agents. *Anal. Bioanal. Chem.* **2017**, *409*, 4915–4926. [[CrossRef](#)] [[PubMed](#)]